Polarized Optical Absorption and Emission Spectra and the Electronic Energy-Level Structure of $Tb(dpa)_3^{3-}$ Complexes in $Na_3[Yb_{0.95}Tb_{0.05}(dpa)_3]\cdot NaClO_4\cdot 10H_2O$†

Todd A. Hopkins, James P. Bolender, David H. Metcalf, and F. S. Richardson*

Department of Chemistry, University of Virginia, Charlottesville, Virginia 22901

Received November 30, 1995⊗

Polarized optical absorption and emission measurements are used to locate and assign 60 crystal-field energy levels split out of the $4f^8$ electronic configuration of Tb^{3+} in single crystals of $Na_3[Yb_{0.95}Tb_{0.05}(dpa)_3]\cdot NaClO_4\cdot 10H_2O$ (where dpa ≡ dipicolinate dianion ≡ 2,6-pyridinedicarboxylate). In these crystals, each Tb^{3+} ion is coordinated to three dipicolinate (dpa) ligands, and the tris-terdentate $Tb(dpa)_3^{3-}$ chelate structures have trigonal-dihedral (D_3) symmetry. The combined optical absorption and emission measurements provide access to the energy-level structures of the 17 lowest-energy $4f^8[SL]J$ multiplet manifolds of Tb^{3+}, and all of these multiplet manifolds are represented among the 60 crystal-field levels that are characterized with respect to both location (energy) and symmetry properties. The energy-level data obtained from experiment are analyzed in terms of a model Hamiltonian that includes consideration of both isotropic and nonisotropic 4f-electron/crystal-field interactions. A parametrized form of this Hamiltonian is used to perform parametric fits of calculated-to-experimental energy-level data, and the results obtained from these data fits show a root mean square (rms) deviation of 10 cm^{-1} between calculated and observed energies. The Hamiltonian parameters evaluated from the energy-level analyses provide information about both the anisotropies and the overall strength of the 4f-electron/crystal-field interactions that contribute to the energy-level structure of $Tb(dpa)_3^{3-}$ complexes. In addition to energy-level data, the polarized emission measurements performed in this study yield information about the relative electric- and magnetic-dipole mechanistic contributions to emission line intensities in the $^7F_J(J=0-6) \leftarrow {}^5D(3)_4$ transition regions of $Tb(dpa)_3^{3-}$, and this information is used to help rationalize the observed chiroptical luminescence properties of enantiomerically resolved $Tb(dpa)_3^{3-}$ complexes in solution.

Introduction

In this paper we report polarized optical absorption and emission measurements on tris(dipicolinate) coordination complexes of terbium(III) in single crystals of *hexagonal* $Na_3[Yb_{0.95}Tb_{0.05}(dpa)_3]\cdot NaClO_4\cdot 10H_2O$ (where dpa ≡ dipicolinate dianion ≡ 2,6-pyridinedicarboxylate). The results obtained from these measurements permit the location and assignment of 60 crystal-field levels split out of the 17 lowest-energy $[SL]J$ multiplet manifolds of the $4f^8(Tb^{3+})$ electronic configuration. These energy-level data are sufficient to support an analysis of the crystal-field interactions that contribute to the $4f^8$ electronic state structure of Tb^{3+} in $Tb(dpa)_3^{3-}$ complexes, and the interaction parameters derived from this analysis are then compared with those determined for other $Ln(dpa)_3^{3-}$ systems.

Both the optical measurements and energy-level analyses reported here for $Tb(dpa)_3^{3-}$ are in kind similar to those reported previously for $Dy(dpa)_3^{3-}$ and $Eu(dpa)_3^{3-}$ complexes in crystalline compounds of stoichiometric formulas $Na_3[Yb_{1-x}Ln_x(dpa)_3]\cdot NaClO_4\cdot 10H_2O$.[1,2] In our previous work on $Dy(dpa)_3^{3-}$, a total of 91 crystal-field levels were located and assigned from a combination of optical absorption and emission measurements,[1] and in our previous work on $Eu(dpa)_3^{3-}$, a total of 52 crystal-field levels were located and assigned.[2] Both the absorption and emission spectra of $Tb(dpa)_3^{3-}$ show line structure that is somewhat more difficult to characterize and assign than that observed for either $Dy(dpa)_3^{3-}$ or $Eu(dpa)_3^{3-}$. This is due, in large part, to the *mixed* electric- *and* magnetic-dipole interaction mechanisms that contribute to many of the transitions observed in the absorption and emission spectra of $Tb(dpa)_3^{3-}$. In several transition regions, line polarization data are of only limited value in making transition assignments (based on symmetry considerations).

The stereochemical properties of $Ln(dpa)_3^{3-}$ complexes and the crystallographic structure of hexagonal $Na_3[Yb(dpa)_3]\cdot NaClO_4\cdot 10H_2O$ host crystals have been described in earlier work[1-3] and will be reviewed only briefly here. The $Ln(dpa)_3^{3-}$ complexes have tris-terdentate chelate structures in which each dpa ligand is coordinated to Ln^{3+} via two carboxylate oxygen donor atoms and a pyridyl nitrogen atom. The LnO_6N_3 coordination polyhedron has a slightly distorted tricapped trigonal prism structure in which oxygen atoms are located at the apices of the trigonal prism and nitrogen atoms are in capping positions. Each of the bicyclic chelate rings in a $Ln(dpa)_3^{3-}$ complex has a 2-fold symmetry axis that coincides with a Ln−N coordination axis, and taken together, the chelate rings form a three-bladed propeller-like structure of trigonal-dihedral (D_3) symmetry. This structure is chiral, with a handedness that reflects the screw sense (or helicity) of the three-bladed propeller assembly. The two enantiomeric forms of this structure are generally labeled as Λ and Δ. In the Λ enantiomer, the propeller assembly has a *left-handed* screw sense about its 3-fold symmetry axis, and in the Δ enantiomer, the propeller assembly has a *right-handed* screw sense about this axis. In aqueous solution, $Ln(dpa)_3^{3-}$ complexes exist as a racemic mixture of rapidly interconverting Λ-$Ln(dpa)_3^{3-}$ and Δ-$Ln(dpa)_3^{3-}$ enantiomers,[4] and they also crystallize as Λ,Δ race-

* Author to whom correspondence should be addressed.
† dpa ≡ dipicolinate dianion (2,6-pyridinedicarboxylate).
⊗ Abstract published in *Advance ACS Abstracts,* August 1, 1996.

(1) Hopkins, T. A.; Metcalf, D. H.; Richardson, F. S. *Inorg. Chem.* **1995**, *34*, 4879.
(2) Hopkins, T. A.; Bolender, J. P.; Metcalf, D. H.; Richardson, F. S. *Inorg. Chem.* **1996**, *35*, 5347.
(3) Albertsson, J. *Acta Chem. Scand.* **1972**, *26*, 1005.
(4) Metcalf, D. H.; Snyder, S. W.; Demas, J. N.; Richardson, F. S. *J. Am. Chem. Soc.* **1990**, *112*, 469.

S0020-1669(95)01525-4 CCC: $12.00 © 1996 American Chemical Society

mates.[3] The chirality-related stereochemical properties of $Ln(dpa)_3^{3-}$ complexes have been exploited extensively in studies of chiral recognition processes in solution media. Among these complexes, $Tb(dpa)_3^{3-}$ has been used most frequently in studies based on luminescence measurement techniques.[5,6]

The $Na_3[Yb(dpa)_3]\cdot NaClO_4\cdot 10H_2O$ host crystals used in the present study have hexagonal symmetry (space group $P\bar{6}2c$ with $Z = 2$),[3] and they can accommodate $Tb(dpa)_3^{3-}$ for $Yb(dpa)_3^{3-}$ substitutions without any apparent changes in crystallographic structure so long as the Tb^{3+}/Yb^{3+} concentration ratio is <0.1. Each of the crystal samples used in the present study was prepared from a solution that contained a 95:5 mole percent ratio of Yb^{3+} to Tb^{3+}.

Experimental Methods

Compound and Crystal Sample Preparation. Hexagonal crystals of $Na_3[Yb_{1-x}Tb_x(dpa)_3]\cdot NaClO_4\cdot 10H_2O$ were grown from aqueous solution following procedures closely similar to those used by Albertsson[3] in the preparation of hexagonal $Na_3[Yb(dpa)_3]\cdot NaClO_4\cdot 10H_2O$ and essentially identical with those used in our previously reported[2] preparation of $Na_3[Yb_{1-x}Eu_x(dpa)_3]\cdot NaClO_4\cdot 10H_2O$ crystals. The mother solution contained 0.95:0.05:3.00 molar ratios of ytterbium perchlorate *to* terbium perchlorate *to* disodium dipicolinate, and the solution was approximately pH 7.5. Morphologically well-defined hexagonal crystals developed from the solution, at room temperature, over a period of weeks, and the crystals harvested for optical studies were typically well-formed hexagonal plates of *ca*. 1 mm thickness. The crystals showed no signs of deterioration during storage under ordinary laboratory atmospheric conditions, and their optical properties remained unchanged over periods of months after their removal from the mother solution.

No attempts were made to determine the exact mole percent ratio of Yb^{3+} to Tb^{3+} ions in the crystals harvested for optical studies, but following arguments similar to those presented in our previous work on $Na_3[Yb_{1-x}Eu_x(dpa)_3]\cdot NaClO_4\cdot 10H_2O$ crystals,[2] it is reasonable to assume that this ratio is close to that of the crystal-growth mother solution (*i.e.*, 95:5). Hereafter, we will use the notation YbTbDPA in referring to the crystals examined in our optical experiments and assume that the composition of these crystals corresponds closely to the stoichiometric formula $Na_3[Yb_{0.95}Tb_{0.05}(dpa)_3]\cdot NaClO_4\cdot 10H_2O$.

The YbTbDPA crystals used in our optical absorption and emission experiments were attached to a one-piece copper mount with Crycon grease and indium foil, and the copper mount was attached to the cold head of a closed-cycle helium refrigerator/cryostat, with strips of indium providing a thermally conductive interface. The crystal samples were attached to the copper mount with their unique (optic) axis aligned either parallel or perpendicular to the direction of light propagation in the optical absorption experiments and the direction of excitation and emission detection in the optical emission experiments. Parallel alignment of the unique axis and the direction of light propagation is referred to here as an *axial* orientation. Perpendicular alignment of the unique axis and the direction of light propagation is referred to as an *orthoaxial* orientation.

In our initial optical experiments, the crystal samples were lightly coated with Crycon grease to inhibit their possible deterioration (via efflorescence) under the high-vacuum conditions in the closed-cycle helium refrigerator/cryostat. However, a repeat of these experiments with unprotected crystal samples yielded essentially identical results, and the crystals showed no signs of deterioration during multiple up-and-down temperature changes (between *ca.* 10 and 293 K) in the cryostat.

Optical Absorption Measurements. All absorption spectra were obtained with a Cary Model 2415 UV−vis-near-IR spectrophotometer. A CTI-Cryogenics closed-cycle helium refrigerator/cryostat, controlled by a Lake Shore Cryotronics temperature-controller (Model DRC-70), was used to achieve a cold-head temperature of 10 K. Absorption spectra were recorded over the 300−500 nm wavelength range. Unpolarized axial and σ- and π-polarized orthoaxial spectra were measured for YbTbDPA crystals. The orthoaxial spectral measurements were taken by fitting a linear polarizing element into the spectrophotometer.

Optical Emission Measurements. Optical emission spectra were measured using instrumentation constructed in this laboratory. An argon-ion laser was used as an excitation source; sample luminescence was dispersed with a 0.75 m double-grating monochromator; and luminescence intensity was measured using photon-counting techniques. In all experiments, sample excitation was along the same direction as emission detection. Two different optical cryostats were used to control sample temperature in the emission experiments. A liquid-nitrogen-cooled cryostat was used in experiments carried out at 77 K. A closed-cycle helium refrigerator was used in experiments carried out at crystal surface temperatures of 10 K, and a continuous-flow liquid-helium cooling system was used in experiments carried out at surface temperatures of 5 K. Analysis of the relative line intensities in these low-temperature experiments indicated that the internal temperature of the crystal was *ca*. 20 K. Single-crystals of YbTbDPA were mounted with their unique (optic) axis aligned either parallel or perpendicular to the direction of emission detection.

For the hexagonal YbTbDPA crystals examined in this study, emission measured along the crystallographic *c*-axis (i.e., unique axis) is unpolarized, and no polarizing (or analyzing) optical elements were used in our axial emission experiments. However, emission measured along a direction that is *perpendicular* to the crystallographic *c*-axis (as in our orthoaxial spectral measurements) can exhibit at least some degree of linear polarization. In our orthoaxial emission experiments, the sample luminescence was analyzed in terms of intensity components polarized perpendicular (σ) and parallel (π) to the crystal *c*-axis. This was done by using a dynamic photoelastic (polarization) modulator that alternately transmitted σ- and π-polarized luminescence intensities to the emission detection unit of our spectrophotometer. The photoelastic modulator (PEM) was a Hinds International Model PEM-80, operated at a modulation frequency of *ca.* 100 kHz.

All of the luminescence observed in our experiments originates from the $^5D(3)_4$ multiplet manifold of Tb^{3+} (centered at *ca*. 20 475 cm^{-1} above ground). The energy gap between this multiplet and the next lower-energy multiplet ($^7F_0$) is *ca.* 14 710 cm^{-1}, which is many times larger than any lattice phonon or molecular vibrational energies in the YbTbDPA crystals. Therefore, nonradiative decay processes for $^5D(3)_4$ are slow, and this multiplet exhibits a strong luminescence. In this study, we measured luminescence spectra throughout the $^7F_J \leftarrow {}^5D(3)_4$ (where $J = 0, 1, 2, 3, 4, 5, 6$) transition regions. For the $^7F_J \leftarrow {}^5D(3)_4$ (where $J = 0-5$) transition regions, the luminescence was excited with the 488.0 nm line of an argon-ion laser, which corresponds to $^7F_6 \rightarrow {}^5D(3)_4$ excitation. The luminescence of the $^7F_6 \leftarrow {}^5D(3)_4$ transition region was excited with UV lines (wavelength range of 351−364 nm) of an argon-ion laser.

Data Analysis

Optical Selection Rules and Line Assignments. The symmetry considerations, selection rules, and types of measurements used for making optical transition assignments in the present study are identical with those used in our previously reported spectroscopic investigation of $Eu(dpa)_3^{3-}$ in single crystals of $Na_3[Yb_{0.95}Eu_{0.05}(dpa)_3]\cdot NaClO_4\cdot 10H_2O$.[2] All crystal-field states split out of the $4f^8(Tb^{3+})$ electronic configuration are assumed to reflect the D_3 point-group symmetry of the $Tb(dpa)_3^{3-}$ complexes in YbTbDPA, and they are labeled

(5) (a) Metcalf, D. H.; Snyder, S. W.; Demas, J. N.; Richardson, F. S. *J. Am. Chem. Soc.* **1990**, *112*, 5681. (b) Metcalf, D. H.; Stewart, J. M.; Snyder, S. W.; Grisham, C. M.; Richardson, F. S. *Inorg. Chem.* **1992**, *31*, 2445. (c) Metcalf, D. H.; Bolender, J. P.; Driver, M. S.; Richardson, F. S. *J. Phys. Chem.* **1993**, *97*, 553. (d) Bolender, J. P.; Metcalf, D. H.; Richardson, F. S. *Chem. Phys. Lett.* **1993**, *213*, 131. (e) Glover-Fischer, D. P.; Metcalf, D. H.; Bolender, J. P.; Richardson, F. S. *Chem. Phys.* **1995**, *198*, 207.

(6) (a) Rexwinkel, R. B.; Meskers, S. C. J.; Riehl, J. P.; Dekkers, H. P. J. M. *J. Phys. Chem.* **1992**, *96*, 1112. (b) Rexwinkel, R. B.; Meskers, S. C. J.; Riehl, J. P.; Dekkers, H. P. J. M. *J. Phys. Chem.* **1992**, *96*, 5725. (c) Rexwinkel, R. B.; Meskers, S. C. J.; Riehl, J. P.; Dekkers, H. P. J. M. *J. Phys. Chem.* **1993**, *97*, 3875. (d) Rexwinkel, R. B.; Meskers, S. C. J.; Riehl, J. P.; Dekkers, H. P. J. M. *J. Phys. Chem.* **1993**, *97*, 13519.

Table 1. Calculated and Experimentally Observed Crystal-Field Energy Levels of Tb^{3+} in Hexagonal $Na_3[Yb_{0.95}Tb_{0.05}(dpa)_3]\cdot NaClO_4\cdot 10H_2O$

				energy (cm^{-1})							energy (cm^{-1})		
level no.	term[a]	J[a]	Γ[b]	calc[c]	expt[d]	Δ[e]	level no.	term[a]	J[a]	Γ[b]	calc[c]	expt[d]	Δ[e]
1	^{7}F	6	A_1	0	0	0	57	^{5}L	10	A_1	26 907	nd	
2	^{7}F	6	E	17	15	2	58	^{5}L	10	A_2	27 028	nd	
3	^{7}F	6	E	59	61	−2	59	^{5}L	10	E	27 029	nd	
4	^{7}F	6	A_1	100	nd		60	^{5}L	10	E	27 037	nd	
5	^{7}F	6	A_2	108	100	8	61	^{5}L	10	E	27 054	nd	
6	^{7}F	6	A_1	132	nd		62	^{5}L	10	A_2	27 075	27 069	6
7	^{7}F	6	E	141	nd		63	^{5}L	10	A_1	27 076	nd	
8	^{7}F	6	A_2	144	nd		64	^{5}L	10	A_1	27 120	nd	
9	^{7}F	6	E	153	161	−8	65	^{5}L	10	E	27 127	27 117	10
10	^{7}F	5	A_1	1 985	1 993	−8	66	^{5}L	10	E	27 155	27 156	−1
11	^{7}F	5	E	2 030	2 034	−4	67	^{5}L	10	A_1	27 170	nd	
12	^{7}F	5	A_2	2 079	2 091	−12	68	^{5}G (3)	5	E	27 694	nd	
13	^{7}F	5	E	2 096	2 107	−11	69	^{5}G (3)	5	A_1	27 704	nd	
14	^{7}F	5	E	2 170	2 183	−13	70	^{5}G (3)	5	E	27 705	nd	
15	^{7}F	5	E	2 270	2 268	2	71	^{5}G (3)	5	A_2	27 707	27 714	−7
16	^{7}F	5	A_2	2 282	2 287	−5	72	^{5}G (3)	5	E	27 722	nd	
17	^{7}F	4	A_1	3 195	3 195	0	73	^{5}G (3)	5	A_2	27 806	27 827	−21
18	^{7}F	4	E	3 308	3 297	11	74	^{5}G (3)	5	E	27 822	27 844	−22
19	^{7}F	4	A_1	3 366	3 364	2	75	^{5}D (3)	2	E	28 084	28 091	−7
20	^{7}F	4	E	3 433	3 423	10	76	^{5}D (3)	2	A_1	28 091	nd	
21	^{7}F	4	A_2	3 465	3 461	4	77	^{5}D (3)	2	E	28 112	28 123	−11
22	^{7}F	4	E	3 591	3 590	1	78	^{5}G (2)	4	E	28 196	28 192	4
23	^{7}F	3	A_1	4 328	4 319	9	79	^{5}G (2)	4	A_1	28 202	nd	
24	^{7}F	3	E	4 352	4 349	3	80	^{5}G (2)	4	A_2	28 220	28 217	3
25	^{7}F	3	E	4 407	4 396	11	81	^{5}G (2)	4	E	28 233	nd	
26	^{7}F	3	A_2	4 418	4 416	2	82	^{5}G (2)	4	A_1	28 238	nd	
27	^{7}F	3	A_2	4 451	4 450	1	83	^{5}G (2)	4	E	28 284	28 271	13
28	^{7}F	2	E	5 026	5 008	18	84	^{5}L	9	E	28 366	nd	
29	^{7}F	2	A_1	5 044	nd		85	^{5}L	9	A_2	28 367	nd	
30	^{7}F	2	E	5 097	5 105	−8	86	^{5}L	9	E	28 393	nd	
31	^{7}F	1	E	5 485	5 475	10	87	^{5}L	9	A_1	28 417	nd	
32	^{7}F	1	A_2	5 529	5 530	−1	88	^{5}L	9	A_1	28 452	nd	
33	^{7}F	0	A_1	5 716	5 739	−23	89	^{5}L	9	E	28 479	28 486	−7
34	^{5}D(3)	4	A_1	20 446	20 450	−4	90	^{5}L	9	A_2	28 498	nd	
35	^{5}D(3)	4	E	20 462	20 461	1	91	^{5}L	9	E	28 510	28 506	4
36	^{5}D(3)	4	A_2	20 476	20 482	−6	92	^{5}L	9	A_2	28 514	nd	
37	^{5}D(3)	4	E	20 477	20 474	3	93	^{5}L	9	E	28 529	nd	
38	^{5}D(3)	4	A_1	20 479	nd		94	^{5}L	9	A_1	28 532	nd	
39	^{5}D(3)	4	E	20 507	20 503	4	95	^{5}L	9	E	28 559	28 563	−4
40	^{5}D(3)	3	A_2	26 059	nd		96	^{5}L	9	A_2	28 571	nd	
41	^{5}D(3)	3	E	26 152	26 163	−11	97	^{5}G (2)	3	A_2	28 877	28 871	6
42	^{5}D(3)	3	A_1	26 188	nd		98	^{5}G (2)	3	E	28 912	28 919	−7
43	^{5}D(3)	3	E	26 206	26 180	26	99	^{5}G (2)	3	E	28 935	nd	
44	^{5}D(3)	3	A_2	26 217	26 207	10	100	^{5}G (2)	3	A_2	28 935	nd	
45	^{5}G(3)	6	E	26 245	26 243	2	101	^{5}G (2)	3	A_1	28 999	nd	
46	^{5}G(3)	6	A_1	26 267	nd		102	^{5}L	8	E	29 132	29 135	−3
47	^{5}G(3)	6	A_2	26 302	nd		103	^{5}L	8	A_2	29 155	nd	
48	^{5}G(3)	6	E	26 303	26 291	12	104	^{5}L	8	E	29 158	nd	
49	^{5}G(3)	6	A_2	26 332	26 347	−15	105	^{5}L	8	A_1	29 173	nd	
50	^{5}G(3)	6	E	26 387	nd		106	^{5}L	8	A_2	29 236	nd	
51	^{5}G(3)	6	A_1	26 442	nd		107	^{5}L	8	E	29 244	nd	
52	^{5}G(3)	6	A_2	26 443	26 446	−3	108	^{5}L	8	A_1	29 254	nd	
53	^{5}G(3)	6	E	26 511	26 486	25	109	^{5}L	8	E	29 271	nd	
54	^{5}L	10	A_2	26 852	26 843	9	110	^{5}L	8	E	29 282	nd	
55	^{5}L	10	E	26 858	26 869	−11	111	^{5}L	8	A_1	29 302	nd	
56	^{5}L	10	E	26 887	nd		112	^{5}L	8	E	29 311	nd	

[a] Identifies the *principal SLJ* components of the eigenvectors. [b] Irreducible representation (irrep) label in D_3 point group. [c] Calculated by using the Hamiltonian parameter values listed in Table 2. [d] Experimentally determined locations of energy levels, with $1/\lambda$(air) to $1/\lambda$(vacuum) corrections included. Uncertainties in the energy-level locations are *ca.* ± 3 cm^{-1} (on average). nd ≡ not determined (*i.e.*, energy level not fully characterized with respect to location and/or symmetry type). [e] Difference between calculated and observed energies.

according to the transformation properties of their state vectors under the symmetry operations of the D_3 point group. These transformation properties are specified by the three irreducible representations (irreps) contained in D_3, which are denoted here by A_1, A_2, and E. Transitions *between* crystal-field levels are classified into six symmetry types: $A_1 \leftrightarrow A_1$; $A_1 \leftrightarrow A_2$; $A_2 \leftrightarrow A_2$; $A_1 \leftrightarrow E$; $A_2 \leftrightarrow E$; and $E \leftrightarrow E$. Electric- and magnetic-dipole selection rules for each of these transition types are discussed and shown explicitly in ref 2.

Energy Level Analysis. The energy-level data obtained in this study were analyzed in terms of a model Hamiltonian that has precisely the same form as that used in our previous work on $Eu(dpa)_3^{3-}$ (see eqs 2−4 of ref 2.). This Hamiltonian assumes D_3 crystal-field symmetry, and it is defined to operate entirely *within* the $4f^8$ electronic configuration of Tb^{3+}. The Hamiltonian includes 26 interaction terms, 20 of which represent spherically symmetric interactions that are largely responsible for the ^{2S+1}L(*term*) and $^{2S+1}L_J$(*multiplet*) structure of the $4f^8(Tb^{3+})$ electronic configuration. The remaining six terms in the Hamiltonian represent non-spherically symmetric crystal-

Table 2. Energy Parameters for the $4f^8$ Electronic Configuration of Tb^{3+} in Hexagonal $Na_3[Yb_{0.95}Tb_{0.05}(dpa)_3]\cdot NaClO_4\cdot 10H_2O$

parameter[a]	value[b] cm^{-1}	parameter[a]	value[b] cm^{-1}
E_{av}	67 882(38)	M^0	4.17(0.06)
F^2	89 508(123)	M^2	$0.56M^0$
F^4	65 337(163)	M^4	$0.38M^0$
F^6	43 025(76)	P^2	[1020]
ζ_{so}	1706(2)	P^4	[510]
α	21.3(0.1)	P^6	[102]
β	−844(4)	B_0^2	−140(23)
γ	1709(23)	B_0^4	−325(42)
T^2	[418]	B_3^4	−365(35)
T^3	[76]	B_0^6	−610(55)
T^4	[79]	B_3^6	−611(38)
T^6	[−323]	B_6^6	−898(26)
T^7	[575]		
T^8	[383]	N[c]	60
		σ[d]	10.0

[a] Defined according to eqs 3 and 4 in ref 2. [b] Determined from parametric fits of the experimentally observed energy-level data listed in Table 1. The numbers shown in parentheses represent uncertainties in the parameter values and correspond to the (±) changes in parameter values that produce a doubling of the *variance* obtained in the data fits. The parameter values shown in square brackets were held fixed in performing the data fits. [c] Number of assigned energy levels included in the parametric data fits. [d] Root mean square deviation between calculated and observed energies (cm^{-1}).

field interactions that can partially remove the $(2J + 1)$-fold degeneracies of J-multiplets and also mix states of different J-multiplet parentage.

As in our previous work on $Eu(dpa)_3^{3-}$, a parametrized form of the model Hamiltonian was used in performing the energy-level calculations reported in the present study. The procedures followed in carrying out these calculations are identical with those described in ref 2, *except* for the number of parameters used as variables in performing calculated-to-experimental energy-level data fits (*vide infra*).

Results and Discussion

Energy Levels. The energy levels located and assigned from our optical absorption and emission measurements on single crystals of YbTbDPA are shown in Table 1, along with a listing of all *calculated* energy levels between 0 and 29 400 cm^{-1}. The levels are characterized with respect to their principal ^{2S+1}L-term and J-multiplet parentages, their crystal-field symmetry label ($\Gamma \equiv A_1$, A_2, or E) in the D_3 point group, and their observed and/or calculated energies. The calculated levels listed in Table 1 were obtained using the Hamiltonian parameter values shown in Table 2. The latter were derived from parametric fits of calculated-to-observed energy-level data. The number of observed levels included in these data fits was 60, and the number of Hamiltonian parameters allowed to freely vary in performing the final data fits was 15. The parameter values shown inside square brackets in the Table 2 listing were held fixed in carrying out the final data fits. These values were arrived at during exploratory data fits in which various subsets of the T^i and P^k parameters were treated as variables. The M^2 and M^4 parameters were constrained according to the relationships: $M^2 = 0.56M^0$ and $M^4 = 0.38M^0$, with M^0 allowed to freely vary. The empirical data set was too small and spanned too few of the $4f^8[SL]J$ multiplet manifolds to permit a thorough exploration of the overall Hamiltonian parameter space.

The results shown in Table 1 span the 17 lowest-energy $[SL]J$ multiplet manifolds of $4f^8(Tb^{3+})$. These multiplet manifolds include a total of 112 crystal-field (Stark) levels, 60 of which are both located and assigned with respect to energy, multiplet parentage, and symmetry properties (in the D_3 point group).

Table 3. Comparison of Crystal-Field Interaction Parameters Determined for $Ln(dpa)_3^{3-}$ Complexes in Single Crystals of Hexagonal $Na_3[Yb_{1-x}Ln_x(dpa)_3]\cdot NaClO_4\cdot 10H_2O$ (Where Ln = Eu^{3+}, Tb^{3+}, or Dy^{3+})[a]

parameter[b]	YbEuDPA[c]	YbTbDPA[d]	YbDyDPA[e]
B_0^2	−272	−140	−198
B_0^4	−103	−325	−394
B_3^4	−433	−365	−643
B_0^6	−483	−610	−663
B_3^6	−1072	−611	−431
B_6^6	−812	−898	−764
S_{cf}^2	122	63	89
S_{cf}^4	207	203	330
S_{cf}^6	544	458	390
S_{cf}	343	292	299

[a] All parameter values are given in units of cm^{-1}. [b] The B_m^k crystal-field parameters are defined according to eq 4 of ref 2. The S_{cf}^k and S_{cf} crystal-field strength parameters are defined according to eqs 1 and 2 in the text. [c] From ref 2. [d] From present work. [e] From ref 1.

The root mean square (rms) deviation between the calculated and observed energies of the 60 assigned Stark levels is 10 cm^{-1}.

Crystal-Field Interaction Parameters. In Table 3, we show a comparison of the crystal-field interaction parameters determined for three different $Ln(dpa)_3^{3-}$ complexes, wherein Ln^{3+} = Eu^{3+}, Tb^{3+}, or Dy^{3+}. All of the B_m^k parameters given in Table 3 are defined according to eq 4 of ref 2, with spherical-tensor normalization properties. The S_{cf}^k and S_{cf} *crystal-field strength* parameters are defined as follows:

$$S_{cf}^{\ k} = \left(\frac{1}{2k+1}[(B_0^{\ k})^2 + 2\sum_{m>0}|B_m^{\ k}|^2]\right)^{1/2} \quad (1)$$

$$S_{cf} = [{}^1/_3\sum_k (S_{cf}^{\ k})^2]^{1/2} \quad (2)$$

The latter parameters provide a measure of the extent to which the non-spherically symmetric components of the crystal-field interactions induce J-level mixings and shift the baricenter energies of J-multiplet manifolds.[7,8]

The results shown in Table 3 reveal that the anisotropies of the 4f-electron/crystal-field interactions are quite different in $Eu(dpa)_3^{3-}$, $Tb(dpa)_3^{3-}$, and $Dy(dpa)_3^{3-}$ complexes, although the *overall* crystal-field strength (S_{cf}) is very similar in these three systems. These results are rather surprising given the essentially identical chemical and structural properties of the ligand environment in the three systems. The relative sizes (ionic radii) of the Ln^{3+} ions in these systems fall in the order $Eu^{3+}(4f^6) > Tb^{3+}(4f^8) > Dy^{3+}(4f^9)$, and each of these ions is larger than the Yb^{3+} ions in the $Na_3[Yb(dpa)_3]\cdot NaClO_4\cdot 10H_2O$ host crystals. It is possible that these differences in Ln^{3+} ionic radii produce small differential distortions in the respective YbEuDPA, YbTbDPA, and YbDyDPA crystal systems and that the observed differences in crystal-field interaction anisotropies are a reflection of these differential distortions. Among the crystal-field strength parameters, one would expect S_{cf}^6 to be the most sensitive to the *shortest-range* Ln^{3+}−ligand interactions, and we note from Table 3 that the values obtained for this parameter fall in the same order as the Eu^{3+}, Tb^{3+}, and Dy^{3+} ionic radii. We also note from Table 3 that the overall (total) crystal-field strength determined for Eu^{3+} in YbEuDPA is *ca.* 16% greater than that determined for Tb^{3+} in YbTbDPA and for Dy^{3+} in YbDyDPA.

(7) Leavitt, R. P. *J. Chem. Phys.* **1982**, *77*, 1661.
(8) Chang, N. C.; Gruber, J. B.; Leavitt, R. P.; Morrison, C. A. *J. Chem. Phys.* **1982**, *76*, 3877.

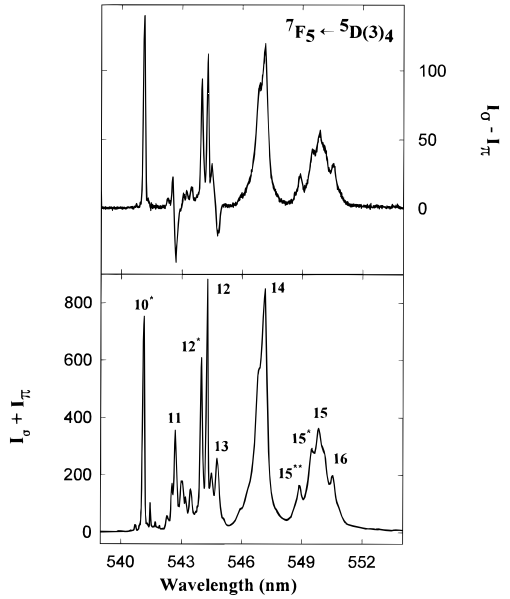

Figure 1. Spectra obtained from linearly polarized, orthoaxial emission measurements in the $^7F_5 \leftarrow {}^5D(3)_4$ transition region of Tb^{3+} in YbTbDPA. The sum ($I_\sigma + I_\pi$) and difference ($I_\sigma - I_\pi$) emission scales are expressed in identical, but otherwise arbitrarily chosen, intensity units. Sample temperature was approximately 20 K. See text for a description of the peak numbering scheme.

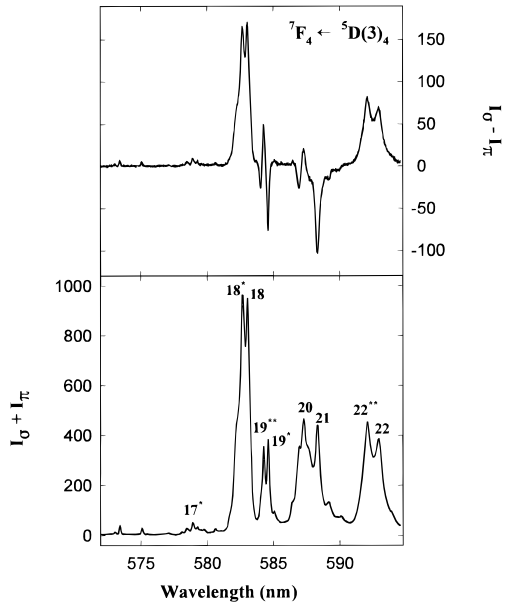

Figure 2. Spectra obtained from linearly polarized, orthoaxial emission measurements in the $^7F_4 \leftarrow {}^5D(3)_4$ transition region of Tb^{3+} in YbTbDPA. The sum ($I_\sigma + I_\pi$) and difference ($I_\sigma - I_\pi$) emission scales are expressed in identical, but otherwise arbitrarily chosen, intensity units. Sample temperature was approximately 20 K. See text for a description of the peak numbering scheme.

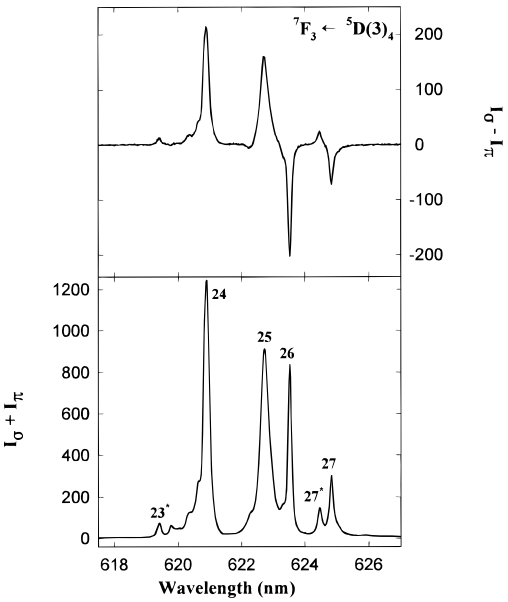

Figure 3. Spectra obtained from linearly polarized, orthoaxial emission measurements in the $^7F_3 \leftarrow {}^5D(3)_4$ transition region of Tb^{3+} in YbTbDPA. The sum ($I_\sigma + I_\pi$) and difference ($I_\sigma - I_\pi$) emission scales are expressed in identical, but otherwise arbitrarily chosen, intensity units. Sample temperature was approximately 20 K. See text for a description of the peak numbering scheme.

Polarized Emission Spectra. The emission spectra of $Tb(dpa)_3^{3-}$ complexes are of considerably greater practical interest than the absorption spectra of these complexes, and in this paper we shall only show examples of spectra obtained from our optical emission measurements. Our emission experiments included measurements of both unpolarized axial and linearly (σ- and π-) polarized orthoaxial emission spectra of YbTbDPA crystals throughout the $^7F_J \leftarrow {}^5D(3)_4$ transition regions of $Tb^{3+}(4f^8)$, which span the 485−690 nm wavelength range. These measurements permitted the location and assignment of all but 5 of the 33 crystal-field levels split out of the $^7F_J(J=0-6)$ multiplet manifolds of $Tb^{3+}(4f^8)$.

Spectra obtained from linearly polarized emission measurements performed on single crystals of YbTbDPA at low temperature (approximately 20 K) are shown in Figures 1−4. These spectra show sums ($I_\sigma + I_\pi$) and differences ($I_\sigma - I_\pi$) of σ- and π-polarized emission intensities measured throughout the $^7F_5 \leftarrow {}^5D(3)_4$, $^7F_4 \leftarrow {}^5D(3)_4$, $^7F_3 \leftarrow {}^5D(3)_4$, and $^7F_{0-2} \leftarrow {}^5D(3)_4$ transition regions of $Tb^{3+}(4f^8)$. The peak (or line) numbers shown in the spectra identify the *terminal* crystal-field levels involved in individual, Stark-level-to-Stark-level transitions (see Table 1 for the energy-level numbering scheme). A single asterisk on a peak number indicates a transition that originates from the first E level of the $^5D(3)_4$ emitting multiplet (level 35 in Table 1), and a double asterisk indicates a transition that originates from the second E level of $^5D(3)_4$ (level 37 in Table 1). Peak numbers *without* asterisks are assigned to transitions that originate from the lowest crystal-field level of $^5D(3)_4$ (level 34 in Table 1), which has A_1 symmetry. For clarity of presentation, only a subset of the lines, peaks, and shoulder features observed in the spectra are given assignment labels in Figures 1−4. The appropriate assignment labels for nearly all the remaining lines and features are easily deduced from comparisons between the spectra and the energy-level data listed in Table 1.

In applications of $Tb(dpa)_3^{3-}$ complexes as optically-active, luminescent probes of chirality-dependent interaction processes in solution, the $^7F_5 \leftarrow {}^5D(3)_4$ transition region (540−552 nm) is of particular interest.[5,6] This transition region not only exhibits the strongest emission intensity but also the strongest *chiroptical activity* observed among the seven $^7F_J \leftarrow {}^5D(3)_4$ multiplet-to-multiplet transition regions of resolved (or partially resolved) $Tb(dpa)_3^{3-}$ complexes. In luminescence spectroscopy, chiroptical activity refers to the differential emission of left- and right-circularly-polarized light by chiral luminophores,[9] and its *strength* is most commonly expressed in terms of *emission dissymmetry factors* defined by $g_{em}(\lambda) = 2[I_L(\lambda) - I_R(\lambda)]/[I_L(\lambda) + I_R(\lambda)]$, where $I_L(\lambda)$ and $I_R(\lambda)$ denote the left (L)- and right

(9) (a) Richardson, F. S.; Riehl, J. P. *Chem. Rev.* **1977**, *77*, 773. (b) Riehl, J. P.; Richardson, F. S. *Chem. Rev.* **1986**, *86*, 1.

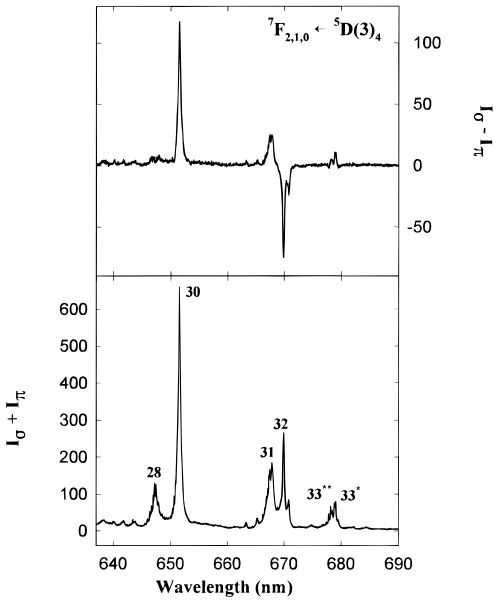

Figure 4. Spectra obtained from linearly polarized, orthoaxial emission measurements in the $^7F_{2,1,0} \leftarrow {}^5D(3)_4$ transition regions of Tb^{3+} in YbTbDPA. The sum ($I_\sigma + I_\pi$) and difference ($I_\sigma - I_\pi$) emission scales are expressed in identical, but otherwise arbitrarily chosen, intensity units. Sample temperature was approximately 20 K. See text for a description of the peak numbering scheme.

(R)-circularly-polarized components of the emission intensity observed at a wavelength λ. For most optically-active luminophores, the observed values of $g_{em}(\lambda)$ are <0.01 (in magnitude) at all emission wavelengths. However, in the $^7F_5 \leftarrow {}^5D(3)_4$ emission region of $Tb(dpa)_3^{3-}$ complexes, the observed values of g_{em} exhibit very large variations (in sign *and* magnitude) with emission wavelength, and at several wavelengths the $|g_{em}|$ values are estimated to be >0.2 for fully- resolved Λ or Δ enantiomers of $Tb(dpa)_3^{3-}$.

The observation of strong chiroptical activity in any given emission region of a chiral luminophore implies that the underlying transitions have substantial electric- *and* magnetic-dipole transition amplitudes with collinear vector components.[9] For an individual transition to exhibit chiroptical activity, it must be both electric- and magnetic-dipole allowed and the scalar product of its electric- and magnetic-dipole transition vectors must be nonvanishing. The YbTbDPA samples examined in the present study do not exhibit any chiroptical luminescence properties because these samples contain a racemic mixture of Λ-$Tb(dpa)_3^{3-}$ and Δ-$Tb(dpa)_3^{3-}$ luminophores. However, the linearly (σ- versus π-) polarized emission measurements performed on these samples provide information about degree of *mixed* electric- and magnetic-dipole character in the different $^7F_J \leftarrow {}^5D(3)_4$ transition regions, and this information is relevant to rationalizing the chiroptical luminescence spectra observed for resolved (or partially resolved) $Tb(dpa)_3^{3-}$ complexes in solution.

Among the seven $^7F_J(J=0-6) \leftarrow {}^5D(3)_4$ multiplet-to-multiplet transition manifolds of $Tb(dpa)_3^{3-}$ in YbTbDPA, only three are predicted by ΔJ selection rules to exhibit any significant magnetic-dipole character in their component, Stark-level-to-Stark-level emission lines. These three transition manifolds are $^7F_3$, $^7F_4$, $^7F_5 \leftarrow {}^5D(3)_4$, among which $^7F_5 \leftarrow {}^5D(3)_4$ is predicted by direct calculations to have the largest magnetic-dipole contributions to transition line strengths.[10] These predictions, based on ΔJ selection rules and on results obtained from direct line-strength calculations, are entirely compatible with the results

(10) Hopkins, T. A. Unpublished results.

Table 4. Polarizations of Emission Lines Observed in the $^7F_{6,5,4,3} \leftarrow {}^5D(3)_4$ Transition Regions of Tb^{3+} in Hexagonal Na_3 [$Yb_{0.95}Tb_{0.05}(dpa)_3$]·$NaClO_4$·$10H_2O$

terminal level[a]					
no.	multiplet	Γ	$\bar{\nu}$[b] cm^{-1}	P[c]	mech[d]
2	$^7F_6$	E	20 435	0.52	ed
3	$^7F_6$	E	20 389	0.50	ed
5	$^7F_6$	E	20 350	0.45	ed
9	$^7F_6$	E	20 289	0.47	ed
11	$^7F_5$	E	18 416	−0.10	md
12	$^7F_5$	A_2	18 359	0.13	md
13	$^7F_5$	E	18 343	−0.08	md
14	$^7F_5$	E	18 267	0.14	ed
15	$^7F_5$	E	18 182	0.15	ed
16	$^7F_5$	A_2	18 163	0.16	md
18	$^7F_4$	E	17 153	0.18	ed
20	$^7F_4$	E	17 027	0.04	ed
21	$^7F_4$	A_2	16 989	−0.23	ed
22	$^7F_4$	E	16 860	0.18	ed
24	$^7F_3$	E	16 101	0.17	ed
25	$^7F_3$	E	16 054	0.17	ed
26	$^7F_3$	A_2	16 034	−0.24	ed
27	$^7F_3$	A_2	16 000	−0.24	ed

[a] Identified according to the level-numbering and labeling scheme used in Table 1. In all cases, the emitting level is the lowest crystal-field level of the $^5D(3)_4$ multiplet (level 34 in Table 1). [b] Observed wavenumber (corrected to vacuum) of the emissive transition. [c] Transition polarization defined by $P = (I_\sigma - I_\pi)/(I_\sigma + I_\pi)$, where I_σ and I_π denote σ-polarized and π-polarized emission intensities obtained in orthoaxial spectral measurements. [d] Dominant transition mechanism. md ≡ magnetic dipole; ed ≡ electric dipole.

obtained from our linearly polarized emission measurements on single crystals of YbTbDPA. All the emission lines observed in the $^7F_{0-2,6} \leftarrow {}^5D(3)_4$ transition regions exhibit strong electric-dipole polarization properties; those observed in the $^7F_{3,4} \leftarrow {}^5D(3)_4$ transition regions exhibit considerably weaker, but still predominantly, electric-dipole polarization properties, but those observed in the $^7F_5 \leftarrow {}^5D(3)_4$ transition region include some that show predominantly electric-dipole polarization properties *and* some that show predominantly magnetic-dipole polarization properties. In Table 4 we show the linear polarization properties observed for a subset of the emission lines that appear in the $^7F_{3-6} \leftarrow {}^5D(3)_4$ transition regions of $Tb(dpa)_3^{3-}$ in YbTbDPA at low temperature. The predominant transition mechanism for each line may be deduced from the sign of the polarization factor, $P = (I_\sigma - I_\pi)/(I_\sigma + I_\pi)$, and an inspection of the electric- and magnetic-dipole selection rules given in Table 1 of ref 2.

The relatively large degree of *mixed* electric- and magnetic-dipole character observed in the $^7F_5 \leftarrow {}^5D(3)_4$ emission lines of $Tb(dpa)_3^{3-}$ provides an explanation for the strong chiroptical activity observed in the $^7F_5 \leftarrow {}^5D(3)_4$ transition region of resolved Λ- or Δ-$Tb(dpa)_3^{3-}$ enantiomers in solution.

Comparisons between Single-Crystal and Solution-Phase Spectra. The results and analysis presented in this paper are based on absorption and luminescence measurements taken on oriented single crystals of $Na_3[Yb_{0.95}Tb_{0.05}(dpa)_3]$·$NaClO_4$·$10H_2O$ at cryogenic temperatures (<80 K). The majority of the studies on $Tb(dpa)_3^{3-}$ complexes that have appeared in the literature have described spectral results obtained on complexes dissolved in aqueous solution, at or near room temperature. A large number of these studies describe chiroptical luminescence results obtained from the $^7F_5 \leftarrow {}^5D(3)_4$ spectral region. One of the incentives for the present work was to rationalize the complex band shape of this spectral region observed in room temperature solution spectra in terms of transitions between crystal-field levels split out of the $^7F_5$ and $^5D(3)_4$ multiplets.

Figure 5 displays luminescence spectra for the $^7F_5 \leftarrow {}^5D(3)_4$ transition region recorded from single crystals of YbTbDPA at

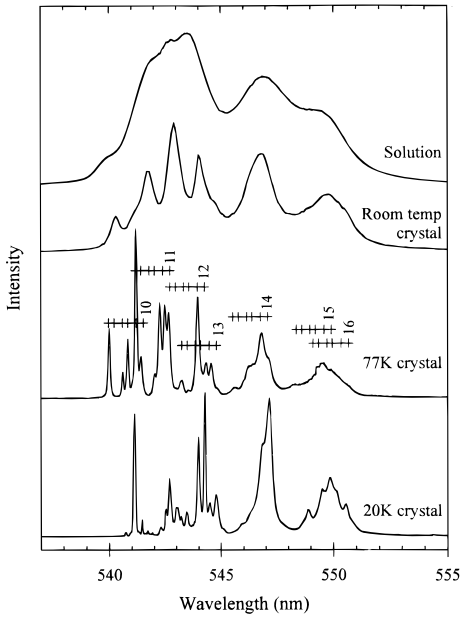

Figure 5. Comparison emission spectra of the $^7F_5 \leftarrow {}^5D(3)_4$ transition region obtained from a crystal of YbTbDPA and from a solution sample of $Tb(dpa)_3^{3-}$ dissolved in H_2O. The crystal spectra were recorded for an orthoaxially mounted crystal at *ca.* 20 K, 77 K, and room temperature and represent sums of σ- and π-polarized emission intensities, while the solution spectrum represents an isotropic emission spectrum. The emission intensity scale is arbitrary and scaled differently for each trace. See text for details.

20 K, 77 K, and room temperature and from an aqueous solution of $Tb(dpa)_3^{3-}$ at room temperature. The crystal spectra were recorded with the crystal mounted in an orthoaxial orientation with respect to the emission detection direction, and each represents the sum of I_σ and I_π intensities observed from the $Tb(dpa)_3^{3-}$ complexes, while the solution sample is *isotropic* with respect to the orientation of the $Tb(dpa)_3^{3-}$ complexes, and the solution spectrum represents the average intensity observed from all possible orientations of the complexes. While the transition intensities expected for isotropic and summed orthoaxial spectra will show some differences, all transitions allowed in the summed orthoaxial spectra will be observed in isotropic spectra, and vice versa. Drawn on the 77 K crystal spectrum are the expected locations of "hot" bands associated with each cold origin assigned from the 20 K spectrum and identified by number corresponding to the terminal level listed in Table 2 (and identified in Figure 1).

Of the 42 possible transitions between the six crystal-field levels of the $^5D(3)_4$ multiplet and the seven crystal-field levels of the $^7F_5$ multiplet, four (the $A_1 \leftarrow A_1$ and $A_2 \leftarrow A_2$ transitions) are strictly forbidden by both electric- *and* magnetic-dipole mechanisms. The other 38 transitions span an energy range of *ca.* 350 cm^{-1}. Broadening of the observed transitions at high temperatures obscures the individual transition locations, but it is apparent that overlapping hot band intensity dominates the spectra at high temperatures. It is also apparent that the solution spectrum is reasonably well-explained in terms of hot-band intensity built upon origins located from the cryogenic crystal spectra.

Conclusion

Solution measurements of luminescence from $Tb(dpa)_3^{3-}$ complexes have been used as a probe for electronic energy-transfer processes,[11] perturbations of the racemic equilibrium existing within $Tb(dpa)_3^{3-}$ populations as a result of added chiral cosolutes or solvents,[12] induction of chiroptical activity into $Tb(dpa)_3^{3-}$ populations as a result of chiral photoselection[13] and, more recently, as a probe for enantioselective energy transfer between an excited-state lanthanide population and resolved optically active transition metal complexes.[4−6] In all of these studies, the $^7F_5 \leftarrow {}^5D(3)_4$ transition region proves the most useful for luminescence measurements, both because of the emission intensity observed in this region and the chiroptical properties of the underlying transitions. In the present study, we have used single-crystal polarized spectroscopy to locate and assign 60 crystal-field energy levels within the 17 lowest-energy $4f^8$-[*SL*]*J* multiplets of Tb^{3+}, including all seven levels within the $^7F_5$ multiplet and five of the six possible levels within the $^5D(3)_4$ multiplet. Location of these levels allows for comparisons to be drawn between solution and crystal luminescence and for some rationalization of both the chiroptical properties and the complex band shapes observed in the solution spectra of $Tb(dpa)_3^{3-}$.

Acknowledgment. This work was supported by the U.S. National Science Foundation (NSF Grant CHE-9213473 to F.S.R.).

IC9515259

(11) Thomas, D. D.; Carlsen, W. F.; Stryer, L. *Proc. Natl. Acad. Sci. U.S.A.* **1978**, *75*, 5746. Wensel, T. G.; Meares, C. F. *Biochemistry* **1983**, *22*, 6247. Meares, C. F.; Wensel, T. G. *Acc. Chem. Res.* **1984**, *17*, 202−209.

(12) Brittain, H. G. *Coord. Chem. Rev.* **1983**, *48*, 243. Wu, S.; Hilmes, G. L.; Riehl, J. P. *J. Phys. Chem.* **1989**, *93*, 2307.

(13) Hilmes, G. L.; Timper, J. M.; Riehl, J. P. *Inorg. Chem.* **1985**, *24*, 1721. Hilmes, G. L.; Riehl, J. P. *Inorg. Chem.* **1986**, *25*, 2617.